J Fluoresc (2015) 25:199–210
DOI 10.1007/s10895-014-1497-6

ORIGINAL PAPER

The Photophysical Properties of Multi-Functional Quantum Dots-Magnetic Nanoparticles—Indium Octacarboxyphthalocyanine Nanocomposite

Charmaine Tshangana · Tebello Nyokong

Received: 1 October 2014 / Accepted: 5 December 2014 / Published online: 17 December 2014

Abstract This work presents the development of a multifunctional hybrid nanoparticle made of $_{L}$-glutathione capped quantum dots (GSH-CdSe@ZnS), amino functionalized Fe_3O_4 magnetic nanoparticles and indium octacarboxy phthalocyanine (ClInPc(COOH)$_8$). In this work we investigate the photophysical properties of the individual components and the hybrid nanoparticle, in addition we study the energy transfer (Förster Resonance Energy Transfer (FRET)) in the complex. FRET efficiencies of ~48 % were obtained for energy transfer between the QDs (when alone or linked to MNPs). Both triplet yields and lifetimes of ClInPc(COOH)$_8$ increase in the nanocomposite, with a decrease in fluorescence lifetime. The hybrid nanoparticle showed improved photophysical properties and as a result can be used in photodynamic therapy.

Keywords Indium octacarboxyphthalocyanine · Quantum dots · Magnetite nanoparticles · Förster resonance energy transfer · Triplet quantum yields

Introduction

In recent years, there has been an increase in research on incorporating diagnostic and therapeutic functions into a single nanoscale system for more effective and improved treatment. Nanoparticles have potential as they are able to achieve dual functions if more than one type of nanostructure can be incorporated into a nano-assembly, which Sailor and Park [1] referred to as a "hybrid nanoparticle". The hybrid nanoparticle is made up of two or more nanoparticles assembled in a functional structure that itself is in nanoscale dimensions [2, 3]. The idea behind the development of hybrid nanoparticles is developing nanosystems that have biomedical properties which are superior to the individual components of the nanosystem.

In this work we develop a hybrid nanoparticle that has potential applications in photodynamic therapy (PDT). The hybrid nanoparticle is made up of $_{L}$-glutathione capped quantum dots (GSH-CdSe@ZnS), amino functionalized Fe_3O_4 magnetic nanoparticles (AMNPs) and indium octacarboxyphthalocyanine (ClInPc(COOH)$_8$). Quantum dots are of interest because they have a broad absorption and narrow emission spectra, size- and composition-tunable emission wavelength. In addition the fluorescence of the QDs can be seen with the naked eye [4–6]. On the other hand, amino functionalized magnetic nanoparticles improve the contrast of magnetic resonance images (MRI), this allows the tumour to be identified non-invasively [7–9]. The final component, a photosensitizer (ClInPc(COOH)$_8$), can accumulate in tumour cells, and upon irradiation with light at a certain wavelength, will result in selective destruction of the tumour cells (through PDT) by generation of cytotoxic singlet oxygen species ($^1O_2$) [10–13].

In this work we first conjugate the GSH-CdSe@ZnS to the AMNPs, then we coat the resulting nanoconjugate with silica. Coating the nanoconjugate with silica preserves optical properties. In addition, silica acts as a potential drug carrier due to the large surface area, tunable size and porosity, chemical stability and biocompatibility [14, 15]. It has been shown that magnetic or fluorescent imaging molecules can be easily coated with silica using well-developed silane and silanol chemistries [16–20]. Quantum dots or magnetic particles coated with a layer of silica have been reported in literature before [21–25]. After coating the GSH-CdSe@ZnS–AMNPs complex with silica, a covalent bond was formed between the resulting complex and the ClInPc(COOH)$_8$, Scheme 1. This was formed by linking the carboxyl of the ClInPc(COOH)$_8$ and the amino group on the surface of the silica. The choice to

C. Tshangana · T. Nyokong (✉)
Department of Chemistry, Rhodes University, Grahamstown 6140, South Africa
e-mail: t.nyokong@ru.ac.za

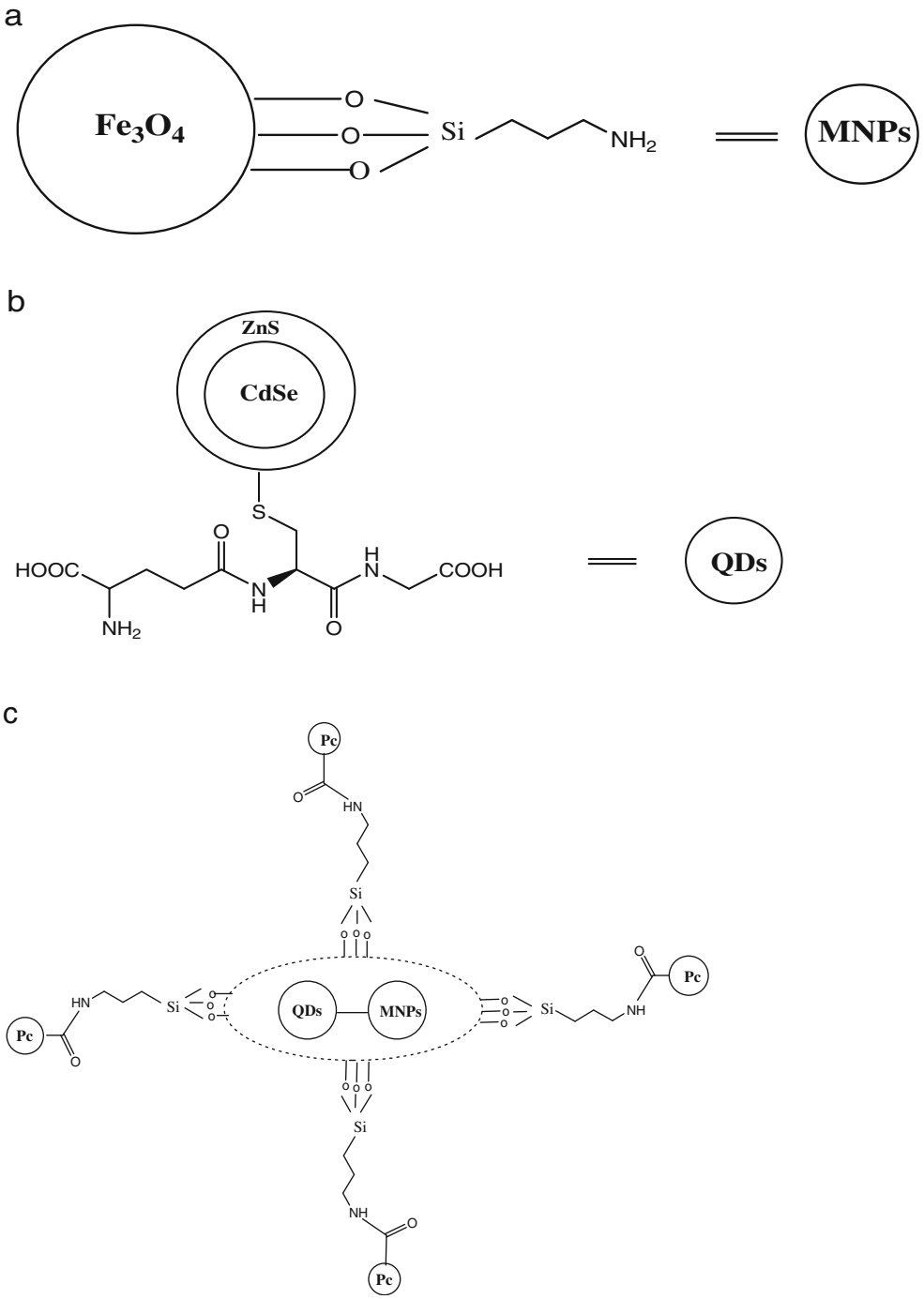

Scheme 1 The individual components of the hybrid nanoparticle are shown above with their corresponding pictorial representation, **a** = amino functionalized Fe_3O_4 magnetic nanoparticles, **b** GSH-CdSe@ZnS QDs and **c** the schematic representation of the covalent linkage of the $ClInPc(COOH)_8$ (Pc) to the silica coated QDs-MNPs

covalently link the $ClInPc(COOH)_8$ instead of entrapping into silica matrix, is because it was reported that drugs can be prematurely released from drug carriers in PDT applications [26]. Hence in recent studies the formation of amide bond between Pcs and silica nanoparticles has been favoured [27, 28]. Apart from our recent report where a composite consisting of MNPs, CdTe QDS and $(OH)AlPc(COOH)_8$ or $ZnPc(COOH)_8$ in the absence of silica nanoparticles [29] was reported, there have been no reports on these types of nano-composites. We compare the photophysical properties of the three in one nanoconjugate with the separate Pc-QDs and Pc-MNPs (Scheme 2).

Experimental

Materials

Dimethylformamide (DMF) was purchased from Merck. N-hydroxysuccinimide (NHS), N-(3-dimethylaminopropyl)-N′-

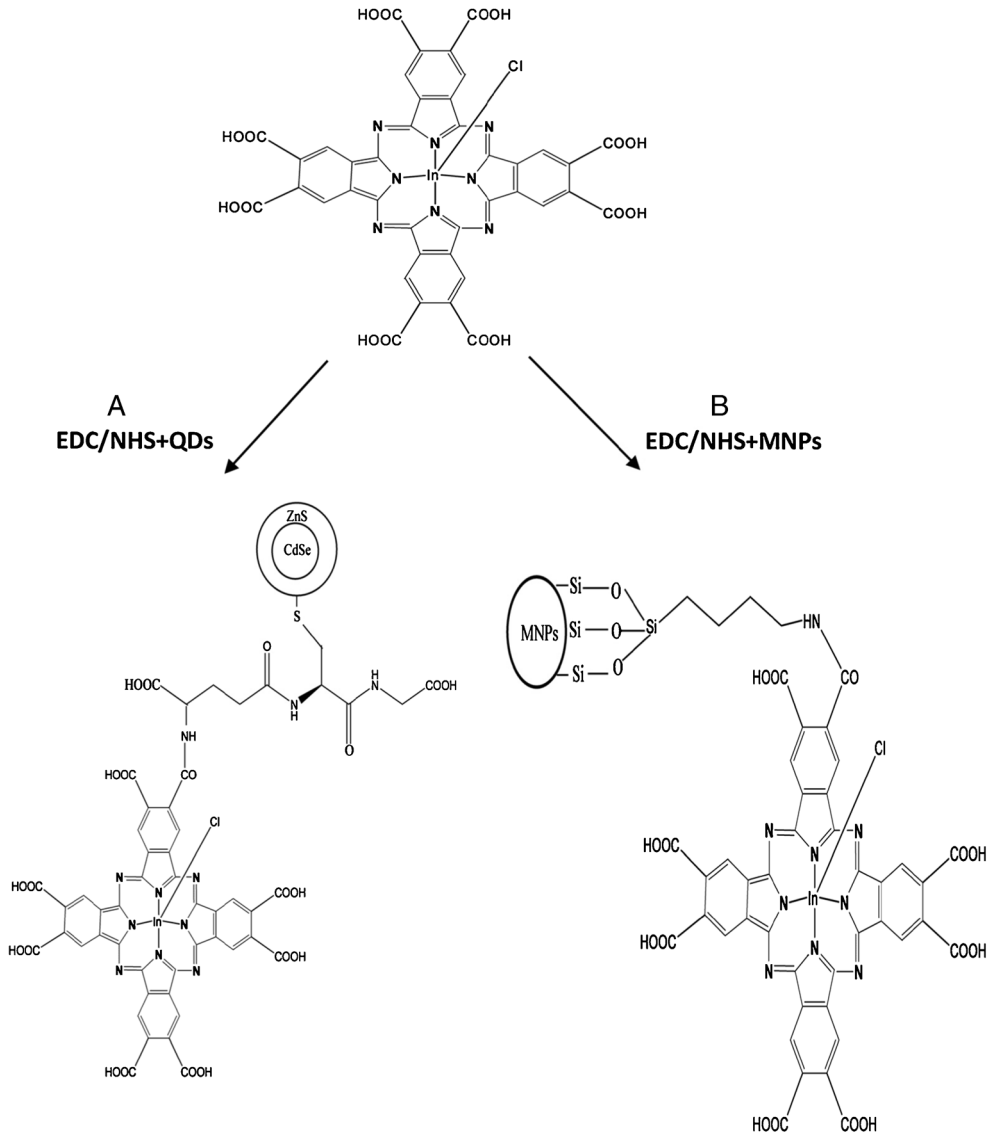

Scheme 2 Schematic representation of the covalent linkage GSH-CdSe@ZnS quantum dots A and MNPs **B** to $ClInPc(COOH)_8$

ethylcarbodiimide hydrochloride (EDC), 3-aminopropyltriethoxysilane (APTES), pyromellitic dianhydride, indium chloride, Triton-X 100, n-hexanol, cyclohexane, tetraethylorthosilicate (TEOS) and NH_4OH and 1, 8-diazabicycloundec-7-ene (DBU) were purchased from Sigma Aldrich. Aqueous solutions were prepared using Millipore water from Milli-Q Water Systems (Millipore Corp, Bedford, MA, USA). Dimethylsulfoxide (DMSO) was obtained from SAARCHEM.

Phosphate buffer saline (PBS) of pH 7.4 were prepared using appropriate amounts of Na_2HPO_4, KH_2PO_4 and respective chloride salts. AlPcSmix (containing a mixture of sulfonated derivatives and used as a standard) was synthesized according to literature methods [30]. GSH-CdSe@ZnS quantum dots were synthesized according to literature methods [31]. The amino functionalized iron oxide (Fe_3O_4) magnetic nanoparticles were synthesized as described before [32].

Equipment

Ultraviolet–visible (UV–Vis) spectra were recorded using Shimadzu UV–Vis 2550 spectrophotometer. The emission spectra were recorded on a Varian Cary Eclipse fluorescence spectrophotometer. Infrared spectra were recorded on Perkin Elmer 100 ART FT-IR spectrometer. Fluorescence lifetimes were measured using correlated single photon counting setup (TCSPC) (PicoQuant FluoTime 200). For QDs fluorescence, the excitation source was a diode laser (LDH-P-C-485 with 10 MHz repetition rate, 88 ps pulse width). For $ClInPc(COOH)_8$ alone or in conjugation, the excitation source was a diode laser (LDH-P-670 driven by PDL 800-B, 670 nm, 20 MHz repetition rate, 44 ps pulse width, Picoquant GmbH). All luminescence decay curves were measured at the maximum of the emission peak and lifetimes were obtained by deconvolution of the decay

curves using the FluorFit Software program (PicoQuant GmbH, Germany).

Mass spectra data were collected with a BrukerAutoFLEX III Smartbeam TOF/TOF Mass spectrometer. The instrument was operated in positive ion mode using a m/z range of 400–3000 amu as described before [33]. The spectra were acquired using alpha-cyano-4-hydroxycinnamic acid as the MALDI matrix, using a 354 nm nitrogen laser.

A laser flash photolysis system was used for the determination of triplet decay kinetics. The excitation pulses were produced by a tunable laser system consisting of an Nd:YAG laser (355 nm, 135 mJ/4–6 ns) pumping an optical parametric oscillator (OPO, 30 mJ/3–5 ns) with a wavelength range of 420–2300 nm (NT-342B, Ekspla).

The kinetic curves were averaged over 256 laser pulses. Triplet lifetimes were determined by exponential fitting of the kinetic curves using OriginPro 8 software. Transmission electron microscopy (TEM) images were obtained using ZESISS LIBRA® 120 transmission electron microscope which operates at 90 kV. X-ray powder diffraction (XRD) patterns were recorded on a Bruker D8, Discover equipped with a proportional counter using Cu-K radiation (=1.5405 Å, nickel filter). Details have been provided before [33]. Using XRD data, the sizes of QDs were determined using the Debye-Scherrer equation (Eq. 1) [34].

$$d = \frac{0.9\lambda}{B\cos\theta} \quad (1)$$

where d is the mean diameter of a quantum dot in nanometers (nm), λ the wavelength of the X-ray source (1.5405 Å), β the full width at half maximum of the diffraction peak and θ, the angular position of the peak.

Synthesis

Covalent Linking of GSH-CdSe@ZnS QDs to Fe_3O_4 Magnetic Nanoparticles

GSH-CdSe@ZnS QDs (10 mg) were dissolved 5 ml of PBS pH 7.4. EDC (0.23 g, 1.2 mmol) and NHS (0.115 g, 1 mmol) were added and the solution stirred for 3 h. The Fe_3O_4 magnetic nanoparticles (5 mg), dissolved in 10 ml of PBS pH 7.4, were added to the activated QDs. The mixture was stirred for 12 h at room temperature under N_2 gas flow. The product was precipitated and washed with ethanol, and centrifuged to remove excess reactants. A magnet was employed to remove un-reacted QDs. The conjugate is represented as QDs-MNPs.

Coating the QDs-MNPs Conjugate with Silica (Scheme 1)

The QDs-MNPs conjugate was coated with silica using methods that have been described in literature [35]. Briefly, a mixture of 1.77 ml of Triton-X 100, 1.8 ml of n-hexanol, 7.5 ml of cyclohexane, 0.48 ml of QDs-MNPs solution (5 mg in 5 ml of PBS pH 7.4), 0.1 ml of TEOS and 6 ml of NH_4OH was stirred for 24 h. After this time, 20 ml of acetone was added followed by centrifuging and washing with ethanol. The resulting conjugate is represented as silica coated QDs-MNPs.

Synthesis of $ClInPc(COOH)_8$

$ClInPc(COOH)_8$ was synthesized according to the methods reported for other octacarboxyphthalocyanines [36, 37] as follows: a mixture of benzene-1, 2, 4, 5-tetracarboxylicdianhydride (pyromelliticdianhydride, 2.50 g, 11.5 mmol), urea (13.0 g, 0.22 mol), $InCl_3$ (23.5 mmol, 5.19 g) and DBU (0.1 g, 0.7 mmol) was heated to 250 °C in a flask until the reaction mixture was fused. The product was washed with water, acetone and 6 M hydrochloric acid. After drying, the product was hydrolyzed in 20 % H_2SO_4 for 72 h. The product was further purified as explained in literature [36, 37].

Yield: (47 %) IR (KBR, cm^{-1}): 3432 (OH) 1716 (C=O) 1381, 1273, 1184 (C–O). ^{1}HNMR (400 MHz, D20): 7.82 ppm (s, 8H, Pc-H) 11.56 PPM (s, 8H carboxylic H). UV–Vis (0.1 M NaoH): lmaxnm (log e), 691 (5.1), 351 (5.5) MS (m/z): Calculated 1014 g/mol Found: 1010 (M+4H). Calculated for $C_{40}H_{16}O_{16}N_8InCl$: C 47.34, H 1.58, N 11.04; Found C 47.57, H 3.70, N 12.47.

Covalent Linking of $ClInPc(COOH)_8$ to Silica Coated QDs-MNPs (Scheme 1)

$ClInPc(COOH)_8$ was covalently linked to silica coated QDs-MNPs as follows: $ClInPc(COOH)_8$ (10 mg) was dissolved in 10 ml dilute NaOH, then 2 ml of 1.2 mM EDC was added to activate the carboxylic group (−COOH) of the Pc. The mixture was allowed to stir for 48 h at room temperature under argon atmosphere. After this time, a mixture containing 2 ml of 1 mM NHS and silica coated QDs-MNPs (0.003 g) was added to the activated Pc and the mixture was stirred for 12 h to allow conjugation of the Pc to the silica coated QDs-MNPs forming Pc-silica coated QDs-MNPs (represented as $ClInPc(COOH)_8$-QDs-MNPs).

Experiments were also performed where QDs or MNPs were individually linked to $ClInPc(COOH)_8$. $ClInPc(COOH)_8$ was covalently linked to GSH-CdSe@ZnS as follows (Scheme 2a): $ClInPc(COOH)_8$ (10 mg, 9.9×10^{-6} mol) was dissolved in 10 ml dilute NaOH, then 2 ml of 1.2 mM EDC was added to activate the carboxylic group (−COOH) of the Pc. The mixture was allowed to stir for 48 h at room temperature under argon atmosphere. After this time, a mixture containing 2 ml of 1 mM NHS and GSH-CdSe@ZnS (0.003 g) was added to the activated Pc, followed by stirring

for 12 h to allow conjugation of the Pc to the QDs to take place. The conjugate is represented as ClInPc(COOH)$_8$-QDs.

For Pc-MNPs conjugate (Scheme 2b): ClInPc(COOH)$_8$ (15 mg, 1.5×10^{-5} mol) was dissolved 5 ml of PBS pH 7.4. EDC (0.23 g, 1.2 mmol) and NHS (0.115 g, 1 mmol) were added and the solution stirred for 3 h. Then Fe_3O_4 magnetic nanoparticles (5 mg, dissolved in 10 ml of PBS pH 7.4), were added to the activated ClInPc(COOH)$_8$. The mixture was stirred for 12 h at room temperature under N_2 gas flow. The product was precipitated and washed with ethanol, and centrifuged to remove excess reactants. A magnet was employed to remove unreacted Pc. The conjugate is represented as ClInPc(COOH)$_8$-MNPs.

Photophysical and Photochemical Parameters

Fluorescence Quantum Yields

The fluorescence quantum yields (Φ_F) were calculated by comparison to a standard using the (Eq. 2) [38]

$$\Phi_F = \Phi_{F(std)}\frac{F.A_{std}.n^2}{F_{std}.A.n_{std}^2} \tag{2}$$

where F and F_{std} are the areas under the fluorescence curves for sample and the standard, respectively. A and A_{std} are the absorbances of the sample and reference at the excitation wavelength respectively, while n and n_{std} are the refractive indices of solvents in which the sample and the reference were dissolved, respectively. Rhodamine 6G standard, dissolved in ethanol, Φ_F=0.95 [39], was employed as a standard for the determination of Φ_F value for QDs. The excitation was at 480 nm for QDs when alone or in the conjugate. For the ClInPc(COOH)$_8$, AlPcSmix standard in aqueous media, Φ_F=0.44 [40] was employed. Excitation was at 665 nm. At this wavelength, there is some minimum absorption from the QDs, which may also be excited. Thus, the values will be used as estimated for the Pc in the presence of QDs. The fluorescence quantum yield values of the QDs after conjugation to ClInPc(COOH)$_8$ ($\Phi_{F(QD)}^{conjugate}$) were obtained using Eq. 3.

$$\Phi_{F(QD)}^{conjugate} = \Phi_{F(QD)}\frac{F_{QD}^{conjugate}}{F_{QD}} \tag{3}$$

where $\Phi_{F(QD)}$ is the fluorescence quantum yield of the QDs alone and used as standard, $F_{QD}^{conjugate}$ is the fluorescence intensity of the QDs in the conjugate with ClInPc(COOH)$_8$ when the excitation wavelength of the QDs (480 nm), $F_{(QD)}$ is the fluorescence intensity of the QD alone at the same excitation wavelength.

Triplet Quantum Yields

Triplet quantum yield values were determined using a comparative method based on triplet decay, using Eq. 4 [41].

$$\Phi_T^{Sample} = \Phi_T^{Std}\frac{\Delta A^{Sample}\varepsilon^{Std}}{\Delta A^{Std}\varepsilon^{Sample}} \tag{4}$$

where A_T^{Sample} and A_T^{Std} are the changes in the triplet state absorbance of the sample (ClInPc(COOH)$_8$ or ClInPc(COOH)$_8$-QDs-MNPs) and the standard, respectively. ε_T^{Sample} and ε_T^{Std} are the triplet state extinction coefficients for the sample (ClInPc(COOH)$_8$, or ClInPc(COOH)$_8$-QDs-MNPs) and standard, respectively. Φ_T^{Std} is the triplet state quantum yield for the standard, Φ_T^{Std}=0.44 for AlPcSmix [40] in aqueous media.

FRET Parameters

FRET efficiency (*Eff*) can be determined from the fluorescence quantum yields of the donor in the absence ($\Phi_{F(QD)}$) and presence ($\Phi_{F(QD)}^{conjugate}$) of the acceptor using Eq. 5 [39]:

$$Eff = 1-\frac{\Phi_{F(QD)}^{conjugate}}{\Phi_{F(QD)}} \tag{5}$$

FRET efficiency (*Eff*) is related to r (Å) by Eq. 6 [39]

$$\mathrm{Eff} = \frac{R_0^6}{R_0^6 + r^6} \tag{6}$$

where r represents the centre-to-centre separation distance (in Å) between the donor and the acceptor, R_0 (the Förster distance, Å) is the critical distance between the donor and the acceptor molecules at which the efficiency of energy transfer is 50 % and depends on the quantum yield of the donor Eq. 7 [39]:

$$R_0^6 = 8.8\times10^{23}\, k^2 n^{-4}\Phi_{F(QDs)}J \tag{7}$$

where k is the dipole orientation factor, n is the refractive index of the medium, $\Phi_{F(QDs)}$ is the fluorescence quantum yield of the donor and J is Förster overlap integral, given by Eq. 8

$$J = \int f_{(QDs)}(\lambda)\varepsilon_{\mathrm{MPc}}(\lambda)\lambda^4\partial\lambda \tag{8}$$

where $f_{(QDs)}$ is the normalized QD emission spectrum. ε_{MPc} and λ are respectively, the molar extinction coefficient and the

wavelength at the Q band maxima for ClInPc(COOH)$_8$. It is assumed that k^2 is 2/3. This assumption is normally made for donor–acceptor pairs in a liquid medium, which are considered to be isotropically oriented during their lifetime. FRET parameters were computed using the program PhotochemCAD [42].

Results and Discussion

Characterization of ClInPc(COOH)$_8$

The synthesis of ClInPc(COOH)$_8$ was achieved using reported methods for other MPc(COOH)$_8$ [36]. Satisfactory UV–vis, IR and NMR spectroscopic as well as elemental analyses were obtained for the complex. The ground state electronic absorption spectra of ClInPc(COOH)$_8$ in 0.1 M NaOH, Fig. 1A(*a*) shows the characteristic monomeric absorption in the Q band region at 691 nm. The monomeric behavior is evidenced by a single narrow Q band typical of metallated phthalocyanine complexes. The emission spectrum (Q band maximum=701 nm), Fig. 1A(*c*) was mirror image of the excitation spectrum (Q band maximum=691 nm) and the latter was similar to the absorption spectrum (Q band maximum=691 nm).

Characterization of the Nanocomposites

UV–Vis Spectra

GSH-CdSe@ZnS QDs were synthesized via previously described methods [31]. Figure 2A shows an overlay of the absorption and emission spectra of the GSH-CdSe@ZnS quantum dots. A broad absorption peak which extends to the near infrared region and a narrow well defined emission are typical for quantum dots, Fig. 2A [43]. The emission and absorption maximum wavelength values for the QDs used in this work are 610 and 586 nm respectively. The fluorescence quantum yield of the QDs was determined to be 0.48 (Table 1), using Eq. 2.

Figure 2B shows the UV–Vis spectra of the (a) amino functionalized Fe_3O_4 magnetic nanoparticles, (b) GSH-CdSe@ZnS QDs and (c) the silica coated QDs-MNPs conjugate. The amino functionalized Fe_3O_4 magnetic nanoparticles show a broad absorption at 385 nm which is typical of magnetic nanoparticles. Upon conjugating the two (QDs and MNPs) an enhanced absorption is noted in the regions where the two absorb.

Figure 1b compares the ground state absorption spectra of ClInPc(COOH)$_8$ and ClInPc(COOH)$_8$-QDs-MNPs. Upon conjugation there is slight shift in the Q-band maxima from

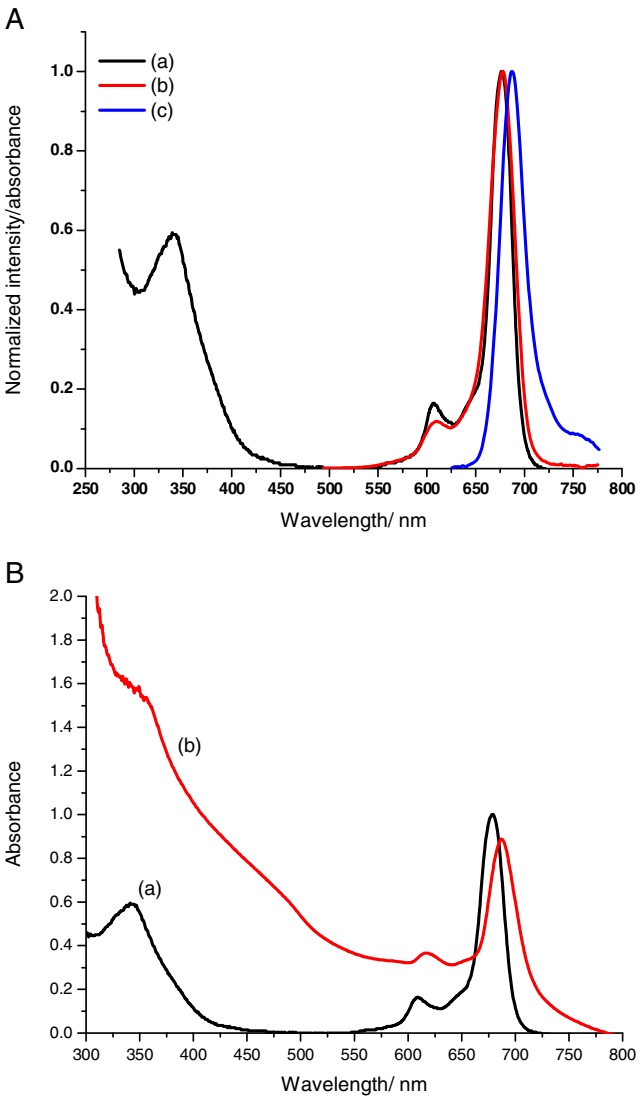

Fig. 1 **A** (*a*) Absorbance, (*b*) excitation and (*c*) emission spectra of ClInPc(COOH)$_8$. **B** Ground state absorption spectra of (*a*) ClInPc(COOH)$_8$ and (*b*) ClInPc(COOH)$_8$-silica coated QDs-MNPs complex

691 nm for ClInPc(COOH)$_8$ to 693 nm for ClInPc(COOH)$_8$-QDs-MNPs. There is also an enhanced absorption below 600 nm region due to the absorption of QDs and MNPs. This indicates successful linkage of the ClInPc(COOH)$_8$ to the silica coated QDs-MNPs complex. There were also no significant spectral changes for ClInPc(COOH)$_8$ in the presence of QDs or MNPs alone, Table 1, apart from the absorption of the latter two (figure not shown).

TEM Images

Figure 3a shows the TEM image of the GSH-CdSe@ZnS QDs, the dots were spherical and well dispersed with no aggregation noted and the size of the individual particles obtained was 2.9 nm. The XRD pattern for GSH-

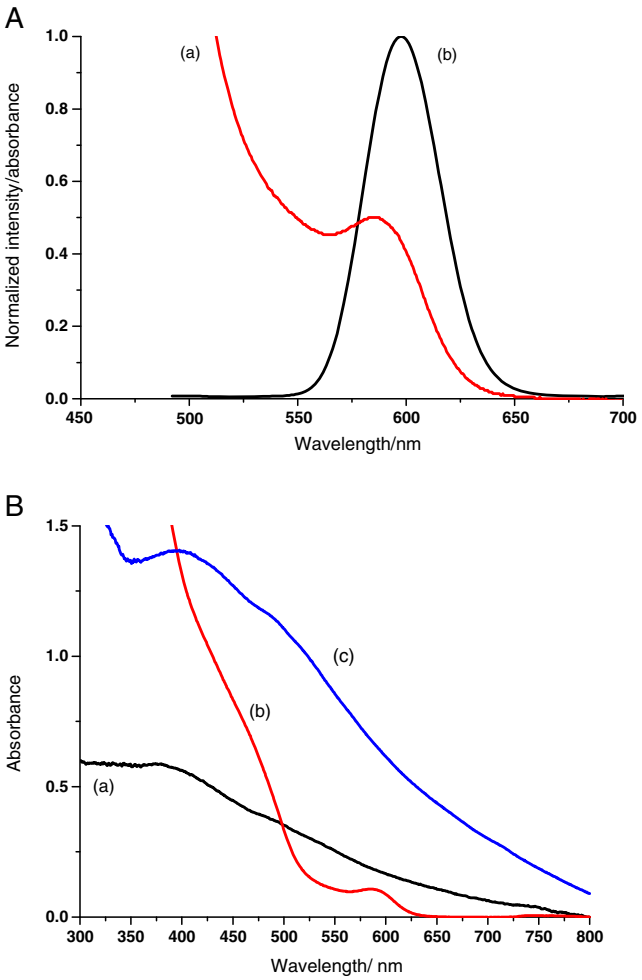

Fig. 2 **A** (*a*) Ground state absorption and (*b*) emission spectra of GSH-CdSe@ZnS in NaOH (O.1 M); **B** Ground state absorption spectra of (*a*) amino functionalized Fe_3O_4 magnetic nanoparticles (MNPs) (*b*) GSH-CdSe@ZnS (QDs) and (*c*) silica coated QDs-MNPs complex

CdSe@ZnSQDs has been reported [31]. The crystalline sizes were determined using the Debye-Scherrer equation. The estimated size obtained from XRD 3.2 nm is which is not too far from the size obtained from TEM. Using TEM, the size of MNPs was determined as 22 nm and they were spherical in nature as seen in Fig. 3b. TEM images of QDs-MNPs shows aggregation making the determination of the individual particle size difficult, Fig. 3c. TEM micrographs obtained in Fig. 3d showed aggregation of the ClInPc$(COOH)_8$-QDs-MNPs conjugate, hence we were unable to determine individual particle sizes using TEM. Using XRD the sizes of the QDs-MNPs-Pc conjugate was determined 82 nm which is not very different from what has been observed in literature for silica coated Fe_30_4 –QDs [44].

FTIR Spectra

In Fig. 4A (a) for the QDs we observe a COO− stretching band at 1591 cm^{-1} and the corresponding –OH band is found around the 3400 cm^{-1} region. Characteristic peaks of primary amino group ($-NH_2$) are observed at 1559 and 1550 cm^{-1} for the amino functionalized Fe_3O_4 magnetic nanoparticles, in Fig. 4A (b). The peak at 1034 cm^{-1} is assigned to Si-O-Si and Fe-O-Si bonding stretch [45]. Successful chemical linkage of MNPs to QDs is confirmed in Fig. 4A (c), as judged by the presence of bands corresponding to primary and secondary amide at 1738 and 1481 cm^{-1}. The encapsulation with the silica was confirmed by the band at 1135 cm^{-1} which is attributed to the Si-O peak.

In Fig. 4B, we compare the FT-IR of the (a) ClInPc$(COOH)_8$ (b) silica coated QD-MNPs conjugate and (c) ClInPc$(COOH)_8$-QDs-MNPs conjugate. In Fig. 4B (a) for the ClInPc$(COOH)_8$, the C=O vibration of the ClInPc$(COOH)_8$ is observed at 1664 cm^{-1}, a broad peak near

Table 1 The photophysical and photochemical parameters of ClInPc$(COOH)_8$, QDs and ClInPc$(COOH)_8$- QDs-MNPs

Complex	$\lambda_{abs(Pc)}$	[a]$\Phi_{F(Pc)}$ (±0.01)	[a]$\Phi_{F(QDs)}$ (±0.01)	[a]$\Phi_{T(Pc)}$	[a, b]$\tau_{F(Pc)}$ (±0.01) (ns)	[a, b]$\tau_{F(QDs)}$ (±0.01) (ns)	[a]$\tau_{T(Pc)}$ (μs)
ClInPc$(COOH)_8$ or QDs alone	691	0.13	0.48	0.49	3.4 (100 %)	26.9 (24 %) 4.3 (31 %) 0.6 (45 %) [8.06]	67
ClInPc$(COOH)_8$-QDs-MNPs	693	0.06	0.33	0.66	3.6 (100 %)	33.8 (22 %) 3.1(38 %) 0.8(40 %) [8.93]	139
ClInPc$(COOH)_8$–MNPs	691	0.10	–	0.61	3.7 (100 %)	–	146
ClInPc$(COOH)_8$-QDs	693	0.09	0.25	0.56	3.3 (100 %)	29.3 (29 %) 3.7(36 %) 0.4(35 %) [9.97]	168

[a] $\Phi_{F(Pc)}$ = fluorescence quantum yield of the Pc (excitation at 665 nm), $\Phi_{F(QDs)}$ = fluorescence quantum yield of the QDs (excitation at 480 nm), $\tau_{F(Pc),}$ = fluorescence lifetime of the Pc, $\tau_{F(QDs)}$ = fluorescence lifetime of the QDs, $\Phi_{T(Pc)}$ = triplet quantum yield of the Pc and $\tau_{T(Pc)}$ = triplet lifetime of the Pc

[b] Abundances in round brackets, and average lifetimes in square brackets

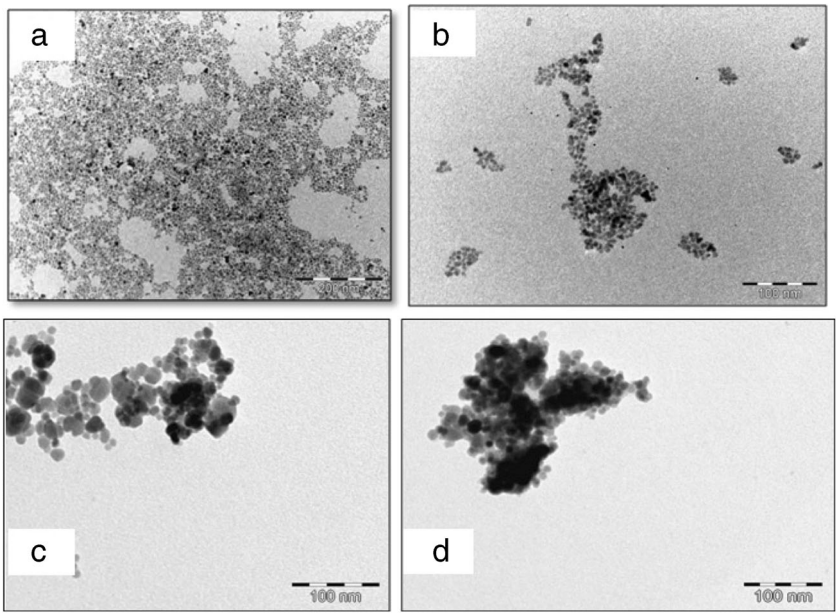

Fig. 3 TEM images of **a** GSH-CdSe@ZnS (QDs), **b** amino functionalized Fe_3O_4 magnetic nanoparticles (MNPs), **c** silica coated QDs-MNPs conjugate and **d** ClInPc(COOH)$_8$-QDs-MNPs conjugate

3250 cm^{-1} corresponds to O–H of the carboxyl groups. The latter broadens upon conjugation with the silica coated QDs-MNPs complex. A peak at 1653 cm^{-1} which corresponds to the amide, confirms the success of the conjugation and the peaks at 971 and 1091 cm^{-1} are attributed to the presence of silica (Fig. 4B (c)).

Photophysical Parameters

Fluorescence Quantum Yields

Luminescence lifetimes were determined using TCSPC. Fitting of the luminescence decay curves for the QDs and

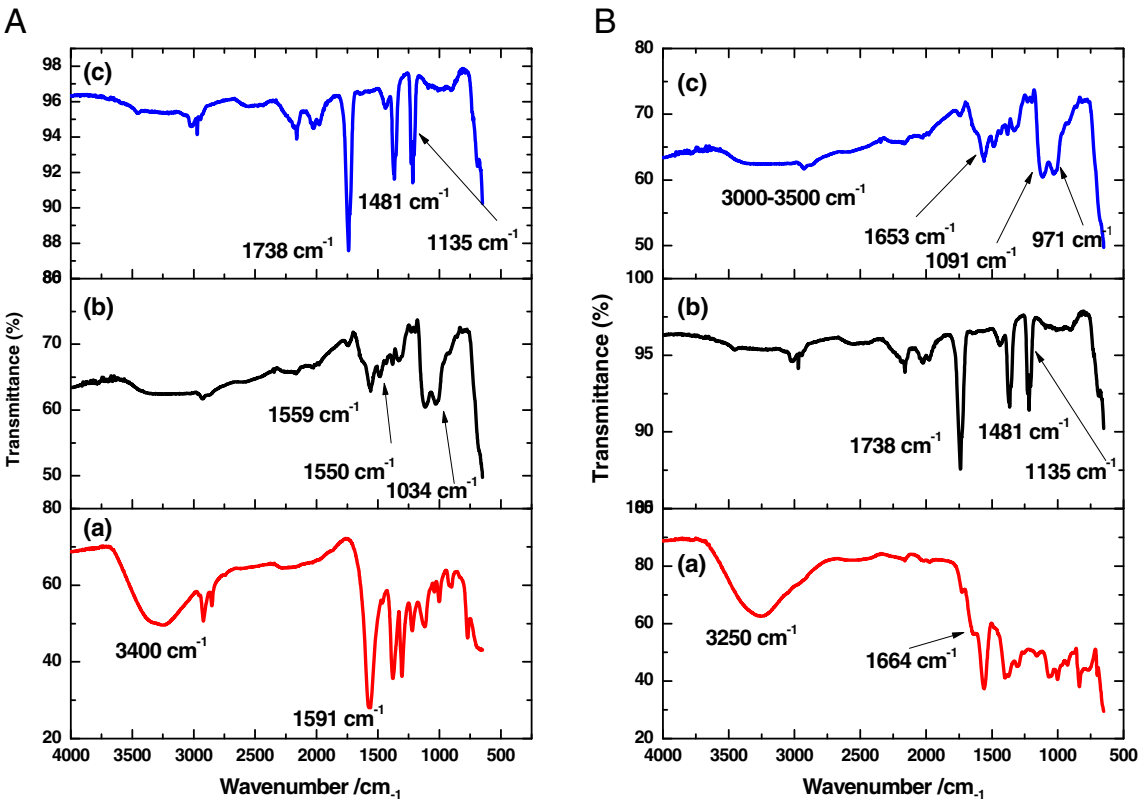

Fig. 4 FT-IR spectra of: **A** (*a*) GSH-CdSe@ZnS QDs (*b*) Amino functionalized Fe_3O_4 magnetic nanoparticles (MNPs) (*c*) silica coated QDs-MNPs, **B** (*a*) ClInPc(COOH)$_8$ (*b*) silica coated QDs-MNPs and (*c*) ClInPc(COOH)$_8$ silica coated QDs-MNPs

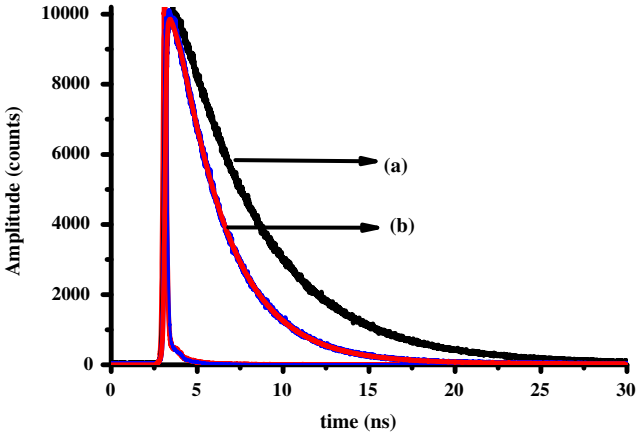

Fig. 5 Fluorescence decay curves of **a** GSH-CdSe@ZnS QDs and **b** ClInPc(COOH)$_8$ silica coated QDs-MNPs

the ClInPc(COOH)$_8$-QDs-MNPs or ClInPc(COOH)$_8$-QDs conjugates resulted in three lifetimes as is typical of QDs [46, 47], While a single lifetime was obtained for both the ClInPc(COOH)$_8$. Fluorescence decay curves of QDs and ClInPc(COOH)$_8$-QDs-MNPs is shown in Fig. 5. There is an increase in the average lifetimes in the presence of the Pc, Table 1, this is surprising since a decrease is expected due to FRET. Though the size of the Pc molecule is smaller than that of the QDs, it is possible that the Pc offers partial protection of the QDs, resulting in the lengthening of the fluorescence lifetime. The fluorescence lifetime of ClInPc(COOH)$_8$ did not change significantly in the presence of MNPs or QDs. When linking the silica coated QDs-MNPs complex to ClInPc(COOH)$_8$ we observed a decrease in the fluorescence quantum yield of ClInPc(COOH)$_8$ (when exciting where Pc absorbs and there is minimal absorption by the QDs). The fluorescence quantum yield decreased from 0.13 (for Pc alone) to 0.06 (ClInPc(COOH)$_8$-QDs-MNPs conjugate) (Table 1). The decrease is as a result of the heavy atom effect of the nanoparticles (QDs and MNPs). The paramagnetic nature of MNPs will also reduce the fluorescence quantum yields. There is also a decrease in fluorescence for ClInPc(COOH)$_8$ when linked individually to MNPs or QDs, Table 1. Due to the enhancement of intersystem crossing (ISC) by the presence of the heavy indium atom, the fluorescence quantum yield of the ClInPc(COOH)$_8$ by itself was low.

We also excited where QDs absorb and Pcs do not. We observed a decrease in the fluorescence quantum yield of QDs in the conjugate (ClInPc(COOH)$_8$-QDs-MNPs), from Φ_F=0.48 for QDs alone to Φ_F=0.33 for the conjugate (Table 1). FRET and other processes which deactivate the excited states of the QDs have been reported to decrease the fluorescence quantum yield [48]. Interestingly when QDs alone are linked to ClInPc(COOH)$_8$, without MNPs, there is a larger quenching of their fluorescence, Table 1, suggesting that the presence of MNPs reduces the surface defects of QDs which result in reduced fluorescence.

Triplet Quantum Yields (Φ_T) and Lifetimes (τ_T)

Nanoconjugates that are to be used in photodynamic therapy applications should be able to populate the triplet excited state and be long lived. The triplet decay curve of the Pc, Fig. 6, obeyed first order kinetics. The Φ_T of the ClInPc(COOH)$_8$-QDs-MNPs conjugate (Φ_T=0.66) was higher than for ClInPc(COOH)$_8$ alone at Φ_T=0.49, Table 1. An increase in Φ_T in the presence of QDs and MNPs is attributed to the combined heavy atom effect of the MNPs and QDs, thus encouraging ISC. The increase in Φ_T suggests that the 3-in one complex (ClInPc(COOH)$_8$-QDs-MNPs) will increase the triplet state population of the phthalocyanine, therefore resulting in enhanced photosensitizing ability. The triplet state quantum yields and lifetimes for ClInPc(COOH)$_8$ increased in all cases in the presence of MNPs, QDs or QDs-MNPs. The largest increase in triplet lifetimes is observed for ClInPc(COOH)$_8$ in the presence of QDs alone, Table 1. The

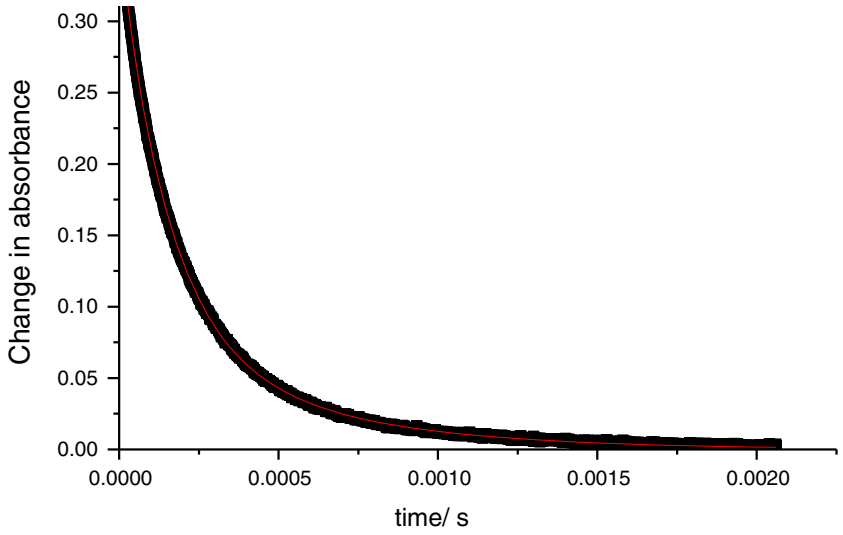

Fig. 6 Triplet Decay profile of ClInPc(COOH)$_8$ in 0.1 M NaOH

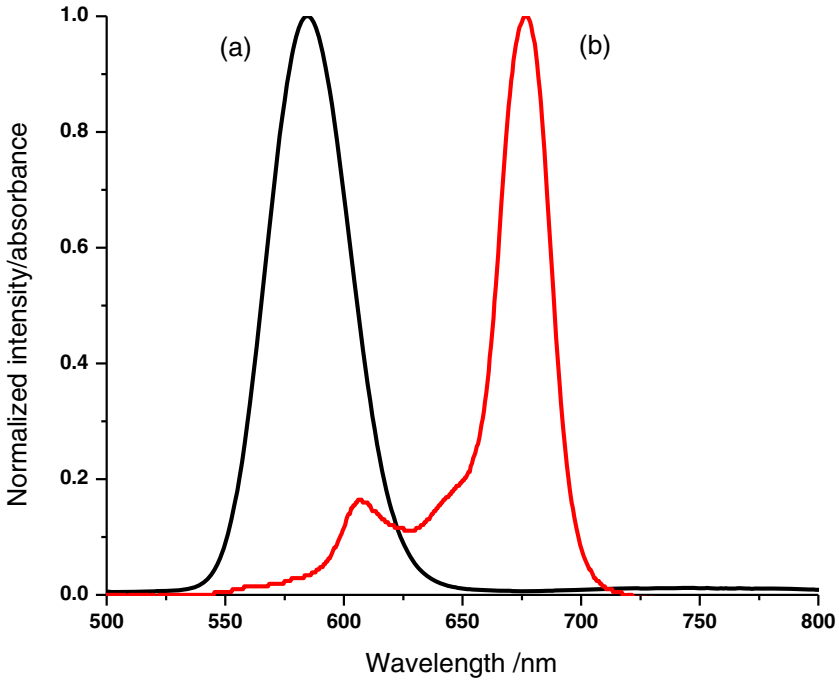

Fig. 7 (**a**) Emission spectra of GSH-CdSe@ZnS (**b**) Ground state absorption spectra of ClIn*Pc* $(COOH)_8$ 0.1 M NaOH

increase in triplet lifetimes suggest that the MNPs, QDs or QDs-MNPs protect the $ClInPc(COOH)_8$ against the environment. Reports on increase in the triplet yields and lifetimes for Pcs in the presence of QDs [49] and other nanoparticles have been documented before.

We also investigated energy transfer between the silica coated QDs-MNPs and the Pc. FRET is a non-radiative energy transfer from an excited donor fluorophore to an acceptor [39]. A good spectral overlap between the fluorescence emission of the QDs with the absorption spectrum of $ClInPc(COOH)_8$ is an important requirement in FRET studies, and the overlap is observed in Fig. 7. FRET occurrence is made evident by the decrease in the photoemission of the donor accompanied by an increase in the acceptors fluorescence. For the $ClInPc(COOH)_8$-QDs conjugate the excitation was carried at 520 nm where QDs absorb but the phthalocyanine does not absorb. An emission peak was observed for the $ClInPc(COOH)_8$ in the $ClInPc(COOH)_8$-QDs-MNPs conjugate which suggests a transfer of energy through FRET from the QDs to ClInPc $(COOH)_8$ (Fig. 8). As stated above, there are other processes which deactivate the excited states of the QDs in addition to FRET, hence a weak stimulated emission

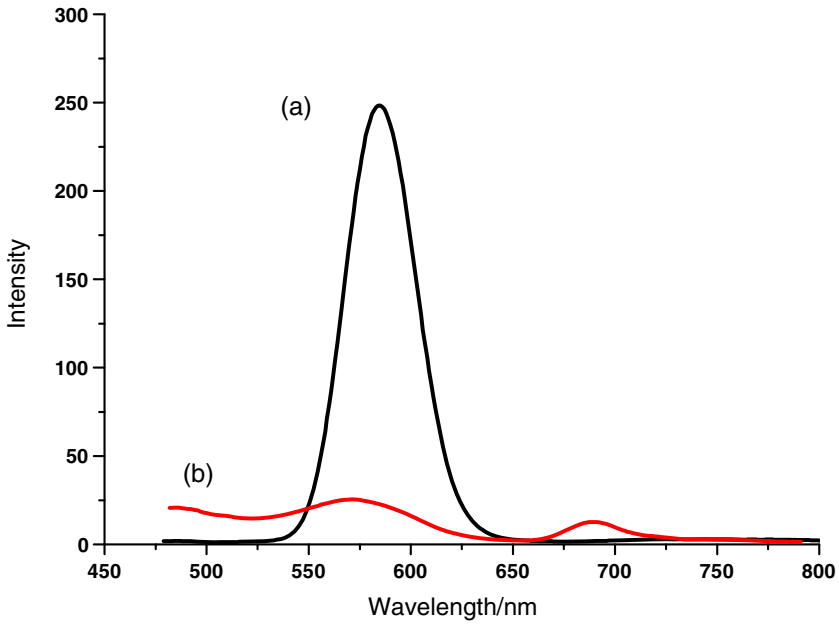

Fig. 8 Fluorescence emission spectra of (**a**) GSH-CdSe@ZnS QDs alone (**b**) $ClInPc(COOH)_8$-QDs-MNPs conjugate

peak is observed in Fig. 8, and the calculated FRET efficiencies *(Eff)* are estimates. The (*Eff)* values was found to be 0.49 for $ClInPc(COOH)_8$-QDs-MNPs, corresponding to R_0 (63.3 Å) being less that r (67.8 Å). For $ClInPc(COOH)_8$-QDs the (*Eff)* values was found to be 0.48 corresponding to R_0 (59.1 Å) being less that r (62.7 Å). The J values obtained in this work were 5.28×10^{14} cm^6 for both the $ClInPc(COOH)_8$-QDs and $ClInPc(COOH)_8$-QDs-MNPs. Thus the value is not different from when QDs alone without MNPs are attached to $ClInPc(COOH)_8$.

Conclusions

The results presented give evidence of a successful synthesis a hybrid nanoparticle ($ClInPc(COOH)_8$-QDs-MNPs conjugate). The conjugate showed improved photophysical properties and we were able to demonstrate a transfer of energy from QDs to Pcs. FRET efficiencies of ~48 % were obtained for energy transfer between the QDs (when alone or linked to MNPs). Both triplet yields and lifetimes of $ClInPc(COOH)_8$ increase in the nanocomposite, with a decrease in fluorescence lifetime. This improved photophysical parameters makes this 3-in-one complex a suitable candidate as a multifunctional drug in PDT applications.

Acknowledgments This work was supported by the Department of Science and Technology (DST) Innovation and National Research Foundation (NRF), South Africa through DST/NRF South African Research Chairs Initiative for Professor of Medicinal Chemistry and Nanotechnology (UID=62620) as well as Rhodes University (South Africa).

References

1. Sailor M, Park J (2012) Hybrid nanoparticles for detection and treatment of cancer. Adv Mater 24:3779–3802
2. Kim J, Park S, Lee J, Jin S, Lee J, Lee I, Yang I (2006) Designed fabrication of multifunctional magnetic gold nanoshells and their application to magnetic resonance imaging and photothermal therapy. Angew Chem Int Ed 46:7754–7758
3. Park J, von Maltzahn G, Ruoslahti E, Bhatia S, Sailor M (2008) Micellar hybrid nanoparticles for simultaneous magneto fluorescent imaging and drug delivery. Angew Chem Int Ed 47:7284–7288
4. Bruchez M, Moronne M, Gin P, Weiss S, Alivisatos A (1998) Semiconductor nanocrystals as fluorescent biological labels. Science 281:2013–2016
5. Chan W, Nie S (1998) Quantum dot bioconjugates for ultrasensitive nonisotropic detection. Science 281:2016–2018
6. Chan W, Maxwell D, Gao X, Bailey R, Han M, Nie S (2002) Luminescent quantum dots for multiplexed biological detection and imaging. Curr Opin Biotechnol 13:40–46
7. Weissleder R, Bogdanov A, Neuwelt E, Papisov M (1995) Long circulating iron oxides for MR imaging. Adv Drug Deliv Rev 16: 321–334
8. Lee J, Huh Y, Jun Y, Seo J, Jang J, Song H, Kim S, Cho E, Yoon H, Suh J, Cheon J (2007) Artificially engineered magnetic particles for ultra-sensitive molecular imaging. Nat Med 13:95–99
9. Park J, von Maltzahn G, Zhang L, Schwartz M, Ruoslahti E, Bhatia S, Sailor M (2008) Magnetic iron oxide nanoworms for tumour targeting and imaging. Adv Mater 20:1630–1635
10. Bonnet R (2002) Chemical aspects of photodynamic therapy. Gordon and Breach Science Publishers, Amsterdam
11. Triesscheijn M, Baas P, Schellens P, Stewart F (2006) Photodynamic therapy in oncology. Oncologist 11:1034–1044
12. Okura I (2001) Photosensitization of porphyrins and phthalocyanines. Gordon and Breach Publishers, Germany
13. Lukyanets E (1999) Phthalocyanines as photosensitizers in the photodynamic therapy of cancer. J Porphyrins Phthalocyanines 3:424–432
14. Pastoriza-Santos L, Perez-Juste I, Liz-Marzán J (2006) Silica-coating and hydrophobation of CTAB- stabilized gold nanorods. Chem Mater 18:2465–2467
15. Sun J, Zhuang J, Guan S, Yang W (2008) Synthesis of robust water-soluble ZnS:Mn/SiO_2 core/shell nanoparticles. J Nanoparticle Res 10:653–658
16. Lai C, Trewyn B, Jeftinija D, Jeftinija K, Xu S, Jeftinija S, Lin V (2003) A mesoporous silica nanosphere-based carrier system with chemically removable CdS nanoparticles caps for stimuli responsive controlled release of neurotransmitters and drug molecules. J Am Chem Soc 125:4451–4459
17. Benezra M, Penate-Medina O, Zanzonico P, Schaer D, Ow H, Burns A, DeStanchina E, Longo V, Herz E, Iyer S, Wolchok J, Larson S, Wiesner U, Bradbury M (2011) Multimodal silica nanoparticles are effective cancer targeted probes in a model of human melanoma. J Clin Invest 121:2768–2780
18. Zhuo X, Kobayashi Y, Romanyuk V, Ochuchi N, Takeda M, Tsunekawa S, Kasuya A (2004) Preparation of silica encapsulated CdSe quantum dots in aqueous solution with improved optical properties. Appl Surf Sci 242:281–286
19. Lin Y, Tsai C, Huang H, Kuo C, Hung Y, Huang D, Chen Y, Mou C (2005) Well ordered mesoporous silica nanoparticles as cell markers. Chem Mater 17:4570–4573
20. Lin Y, Hung Y, Su J, Lee R, Chang C, Lin M, Mou C (2004) Gadolinium(III)-incorporated nanosized mesoporous silica as potential magnetic resonance imaging contrast agents. J Phys Chem B 108(40):15608–15611
21. Gerion D, Pinaud F, Williams S, Parak W, Zanchet D, Weiss S, Alivistos A (2001) Synthesis and properties of biocompatible water soluble silica coated CdSe/ZnS semiconductor quantum dots. J Phys Chem B 105:8861–8871
22. Philipse A, van Bruggen M, Pathmamanoharan C (1994) Magnetic silica dispersions: preparation and stability of surface-modified silica particles with a magnetic core. Langmuir 10:92–99
23. Bechger L, Koenderink A, Vos W (2002) Emission spectra and lifetimes of R6G dye on silica coated titania powder. Langmuir 18: 2444–2447
24. Wolcott A, Gerion D, Visconte M, Sun J, Schwartzberg A, Chen S, Zhang J (2005) Silica-coated CdTe quantum dots functionalized with thiols for bioconjugation to IgG proteins. J Phys Chem B 110:5779–5789
25. Selvan S, Tan T, Ying J (2005) Robust, non-cytotoxic, silica coated CdSe quantum dots with efficient photolumiscence. Adv Mater 17: 1620–1625
26. Lin R, Zhou L, Lin Y, Wang A, Zhou J, Wei S (2011) Property study of a new silica nanoparticle delivery system of hydrophobic phthalocyanine using spectroscopic method. Spectroscopy 26:179–185
27. Fashina A, Antunes E, Nyokong T (2013) Enhanced photophysical behavior of phthalocyanine when grafted on silica nanoparticles. Polyhedron 53:278–285
28. Wang F, Chen X, Zhao Z, Tang S, Huang X, Lin C, Cai C, Zheng N (2011) Synthesis of magnetic, fluorescent and mesoporous core-shell-structured nanoparticles for imaging, targeting and photodynamic therapy. J Mater Chem 21:11244–11252

29. Idowu M, Nyokong T (2012) Photophysical behaviour of fluorescent nanocomposites of phthalocyanines linked to quantum dots and magnetic nanoparticles. Int J Nanosci 11:1250018-1–1250018-9
30. Ambroz M, Beeby A, McRobert A, Simpson M, Svensen R, Phillips D (1991) Preparative, analytical and fluorescence spectroscopic studies of sulphonated aluminium phthalocyanine photosensitizers. J Photochem Photobiol B Biol 9:87–95
31. Adegoke O, Nyokong T (2014) Conjugation of monosubstituted phthalocyanine deravitives to CdSe@ZnS quantum dots and their applications in fluorescence sensing. Synth Met 188:35–45
32. Modisha P, Nyokong T, Antunes E (2013) Photodegradation of Orange-G using zinc octacarboxyphthalocyanine supported on Fe3O4 nanoparticles. J Mol Catal A Chem 380:131–138
33. Masilela N, Nyokong T (2011) Conjugates of low symmetry carboxy Ge, Sn and Ti pthalocyanine with glutathione capped gold nanoparticles: an investigation of photophysical properties. J Photochem Photobiol A 223:124–131
34. Sapra S, Sarma D (2005) Simultaneous control of nanocrystal size and nanocrystal-nanocrystal in CdS nanocrystal assembly. Pramana 65:565–570
35. Bagwe R, Yang C, Hilliard L, Tan W (2004) Optimization of dye doped silica nanoparticles prepared using reserve microemulsion method. Langmuir 20:8336–8342
36. Sakamoto K, Ohno E (1997) Synthesis and electron transfer of phthalocyanine derivatives. Prog Org Coat 31:139–145
37. Masilela N, Idowu M, Nyokong T (2009) Photophysical, photochemical and electrochemical properties of water soluble silicon, titanium and zinc phthalocyanines. J Photochem Photobiol A Chem 201: 91–97
38. Fery-Forgues S, Lavabre D (1999) Are fluorescence quantum yields so tricky to measure? A demonstration using familiar stationery products. J Chem Int Ed 76:1260–1264
39. Lakowiecz J (1999) Principles of fluorescence spectroscopy, 2nd edn. Kluwer Academic/Plenum Publishers, New York
40. Ogunsipe A, Nyokong T (2005) Photophysical, photochemical and bovine serum albumin studies on new gallium (III) phthalocyanine. J Photochem Photobiol Sci 4:510–516
41. Kubat P, Monsinger J (1996) Photophysical properties of metal complexes of meso-tetrakis(4-sulphonatophenyl)porphyrin. J Photochem Photobiol A 96:93–97
42. Du H, Fuh R, Li J, Cockan L, Lindsey J (1998) PhotochemCAD: a computer aided design and research tool in photochemistry. Photochem Photobiol 68:141–142
43. D'Souza S, Antunes E, Litwinski C, Nyokong T (2011) Photophysical behavior of zinc monoamino phthalocyanine linked to mercaptopropionic acid capped CdTe quantum dots. J Photochem Photobiol A 220:11–19
44. Guo J, Yang W, Wang C, He J, Chen J (2006) Poly (N-isopropylacrylamide)-coated luminescent/magnetic silica microspheres: preparation, characterization and biomedical applications. Chem Mater 18(23):5554–5562
45. Oliveria D, Macaroff P, Ribeiro K, Lacava R, Azevedo R, Lima E, Morais P, Tedesco A (2005) Studies of zinc phthalocyanine/magnetic fluid complex as bifunctional agent for cancer treatment. J Magn Magn Mater 289:476–479
46. Wang X, Qu L, Zhang L, Peng X, Xiao M (2003) Surface-related emission in highly lumiscent CdSe quantum dots. Nano Lett 3:1103–1110
47. Sun X, Chen J, Song J, Zhao D, Deng W, Lei W (2010) Ligand capping effect for dye solar cells with CdSe quantum dots sensitized ZnO nanorod photoanode. Opt Express 18:129–1301
48. Zenkevich E, Stupak A, Kowerko D, von Borczyskowski C (2012) Influence of single dye molecules on temperature and time dependent optical properties of CdSe/ZnS quantum dots: ensemble and single nanoassembly detection. Chem Phys 406:21–29
49. Moeno S, Nyokong T (2008) The photophysical studies of a mixture of CdTe quantum dots and negatively charged zinc phthalocyanine. Polyhedron 27:1953–1958